

# Generalizable Imitation Learning Through Pre-Trained Representations

Wei-Di Chang<sup>1</sup>, Francois Hogan<sup>1</sup>, David Meger<sup>1</sup>, and Gregory Dudek<sup>1</sup>

**Abstract**—In this paper we leverage self-supervised vision transformer models and their emergent semantic abilities to improve the generalization abilities of imitation learning policies. We introduce BC-ViT, an imitation learning algorithm that leverages rich DINO pre-trained Visual Transformer (ViT) patch-level embeddings to obtain better generalization when learning through demonstrations. Our learner sees the world by clustering appearance features into semantic concepts, forming stable keypoints that generalize across a wide range of appearance variations and object types. We show that this representation enables generalized behaviour by evaluating imitation learning across a diverse dataset of object manipulation tasks. Our method, data and evaluation approach are made available to facilitate further study of generalization in Imitation Learners.

## I. INTRODUCTION

Once humans acquire a manipulation skill, they are able to immediately adapt it to unseen objects despite drastic variation in visual appearance and geometry. This is perhaps due to the human ability to identify operational concepts, such as seats or handles. Learned robotic behaviours, on the other hand, typically do not generalize beyond their training data.

In this paper, we consider the setting of imitating manipulation policies for objects which are *unseen* in the training set. Imitation Learning (IL) is a proven method for training complex robot behaviours from demonstrations. It offers better sample efficiency than learning behaviours from scratch through Reinforcement Learning (RL) and avoids the need to engineer a reward function [1]–[5]. However, despite these successes, IL often relies on limited distribution shift, where the training dataset closely matches the final evaluation.

Leveraging pre-trained visual representations is a common solution to sample efficiency and generalization. Prior work has shown their benefits in control and IL [6]–[8]. Using pre-trained representations also comes with the benefit of improved generalization that may be achieved through training on larger more diverse training datasets. Recent visual representation learning methods have impressively shown such semantic and generalization abilities. In particular, self-supervised approaches such as DINO exhibit zero-shot emerging abilities such as background-foreground segmentation [9] and encode semantic object-part information in its embeddings [10]. We show in Figure 1 an example of the zero-shot abilities DINO Vision Transformers (ViTs) representations afford on the objects used in our experiments,

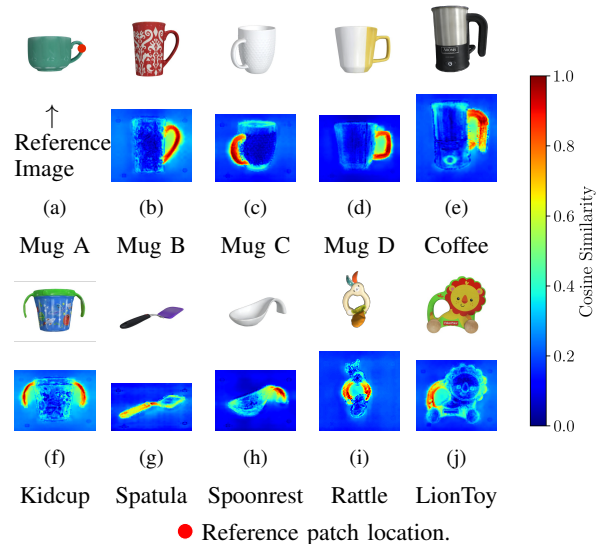


Fig. 1: **DINO ViT embeddings encode zero-shot fine-grained part-semantic information.** Cosine Similarity heatmap between DINO image patch embeddings of various household objects and reference patch, all previously unseen. 10 of the 24 objects from the Google Scanned Objects dataset<sup>2</sup> [11] used in our manipulation experiments to test the generalization abilities of IL policies.

extracting out parts of objects with the same semantics using just cosine similarity, although never having been trained or fine-tuned on this particular dataset. Exploiting these rich and well-localized general representations should therefore result in more generalizable visuomotor policies.

Our first contribution is to build a set of benchmark tasks using the Google Scanned Objects dataset [11] that tests the ability of IL algorithms for robotic manipulation to generalize under two challenging settings: within a class when the manipulated objects changes in both visual appearance and morphology, and across classes, with objects of vastly different appearance and morphology. To train the IL agents, we collect a dataset of expert demonstrations through teleoperation. Our benchmark is designed to study these generalization facets of IL independently and measure how transferable policies learnt through imitation are to novel, unseen objects.

Our second contribution is to introduce BC-ViT, an imitation learning algorithm that leverages rich DINO pre-trained ViT patch-level embeddings to obtain better generalization

<sup>2</sup>Images of 3D Scanned Household Items by Laura Downs and Anthony Francis are licensed under a Creative Commons Attribution 4.0 International License (<https://creativecommons.org/licenses/by/4.0/>) at (<https://research.google/resources/datasets/scanned-objects-google-research/>)

<sup>1</sup>Samsung AI Center Montréal, Samsung Research, Montréal, Canada. {w.chang1, d.meger}@partner.samsung.com, {f.hogan, g.dudek}@samsung.com.

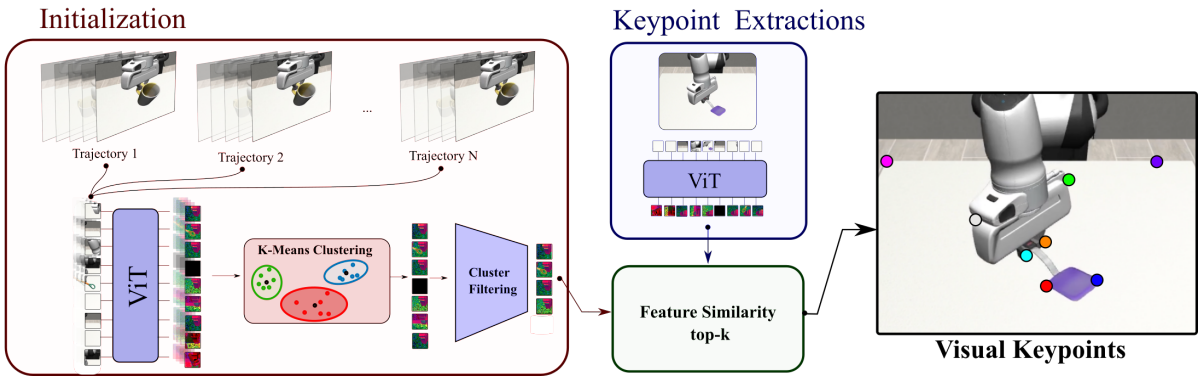


Fig. 2: **Overview of our feature extraction pipeline.** Through K-Means clustering our approach extracts reference DINO features that represent specific semantic concepts from the demonstration dataset. These reference features are used in downstream policy learning, to abstract images seen in rollouts into semantic visual keypoints.

when learning from demonstrations. Across the increasingly difficult cases of our benchmark, BC-ViT shows improved transfer of the learnt manipulation policy to unseen objects when compared to state-of-the-art IL approaches. To facilitate reproducibility, all of our code, for both the method and the benchmark will be open-sourced.

## II. RELATED WORK

**IL for Manipulation** Learning manipulation behaviours from demonstrations has been widely studied, where most methods broadly fall within the categories of Inverse Reinforcement Learning [1] and Imitation Learning (IL). Behaviour Cloning (BC) [12] remains a widely used approach due to its simplicity and its performance in real-world settings [13]–[15], despite its well-known shortcomings [16]. Various policy functional forms have been proposed to improve the spatial generalization and ability to handle system dynamics [4], [5]. Our work is motivated by the development of policies that generalize to a large variety of environments, while being trained on limited supervised interactions.

In [15], the Robomimic simulation environment is introduced and presents an extensive benchmark study of BC variants. One widely adopted design decision [17]–[19] throughout visuomotor policy learning to yield better generalization is the use of Spatial Softmax layers at the output of a CNN backbone, shown to enable the abstraction of the convolutional features into a vector of 2D image coordinates [20]. Our keypoint extraction approach is reminiscent of the image coordinate abstraction of Spatial Softmax Layers, but adapted for ViTs. The main advantage of our approach is that the extracted keypoints lead to a consistent semantic concept attached to each extracted 2D coordinate.

**Pre-trained Representations for Control and IL** Leveraging pre-trained embeddings has been shown to improve the performance and data efficiency of visual control policies in many instances. CURL [21], and other related methods [22]–[24], use a combination of image augmentations, contrastive losses, or estimates of the dynamics to train a representation, enabling state-of-the-art performance on locomotion benchmark tasks. In these approaches, the representations are learnt

from data collected in the testing environment, as opposed to being trained on general purpose datasets, lowering the potential for transfer to novel environments. Parisi et al. [6] studies the transferability of representations pre-trained on general purpose image datasets such as Imagenet [25] for visual control tasks, and find that these representations can even outperform ground-truth state representations. In the realm of self-supervised approaches, R3M [7] and MVP [8] use general purpose datasets, similarly to our approach. R3M uses time contrastive learning, video-language alignment, and a sparsity penalty on the Ego4D dataset [26], showing improvements on IL tasks through the use of their pre-trained representation. MVP [8] is the closest approach to ours, which consists in pre-training a ViT-based Masked Auto Encoder (MAE) on Imagenet and using its compact image-level output of ViT, the [CLS] token, to obtain performance improvements when applied to RL with some transferability to novel objects. Our experimental results show that our method outperforms both of these approaches.

In contrast with MVP, we propose to use the dense patch-level ‘key’ embeddings of DINO pre-trained ViTs, as described in [10], for their part-based semantic abilities. These embeddings are better localized and following our keypoint extraction method, better abstracted by preventing any potential overfitting to specific features. Figure 1 shows the zero-shot abilities of DINO embeddings, extracting semantic parts of objects using just cosine similarity over the patch embeddings.

**Object Generalization in Control** Domain randomization is a common method to address noise and shifts in visual sensing [27], [28]. In this paper, we are motivated by the insight that humans are capable of abstraction over not only the appearance, but the shape of objects and the class. Object-abstraction in control has previously often relied on either bounding boxes [29]–[32], or pose estimation [33]–[35]. Dense Object Net [36] learns dense image representations through self-supervised robot interaction and a dense correspondence loss, enabling precise keypoint localization on objects of the same class. In contrast with previous

approaches, BC-ViT extracts visual object-part semantic concepts from the expert demonstration and tracks these semantic concepts as keypoints, perceiving each object as a configuration of keypoints. Importantly, our method avoids the rigidity of bounding boxes and does not require any supervision or environment interaction during the training of the representation.

### III. BACKGROUND

**Vision Transformers** The ViT architecture encodes a sequence of input patches into a sequence of patch embeddings through a self-attention mechanism. From an image input as a grid of non-overlapping patches, each patch is first flattened and embedded through a linear projection. Multi-Head Self-Attention (MHSA) is then applied to this sequence of patch linear embeddings. Multiple MHSA layers are stacked, along with alternating feedforward layers to learn useful representations of the input patches. ViTs maintain the size of the feature map across layers, as opposed to CNN-based architectures which reduce the feature map through pooling layers. While this provides fine-grained patch-level feature localization throughout, even with small architectures, ViTs can have prohibitively large output sizes at the patch-level. Subsequent modifications [10] extract overlapping image patches by striding the patches over the image, resulting in even finer feature location resolution and a larger output size.

Extracting features from ViTs can be done in multiple ways. One approach is to add a class [CLS] token to the sequence of input patches, using its output [CLS] as a global embedding of the image [37]. This compact image-level [CLS] embedding is often used for downstream tasks [8], sidestepping the issue of the large output size of the full ViT embedding but at the cost of ignoring the dense patch-localized embeddings entirely. Pooling the patch embeddings and concatenating them to the [CLS] token is another approach [9]. Although methods exist for reducing the high dimensionality of ViT patch-level outputs [9], [38], [39], these methods have poor applicability to our goal of generalization, as they lose localization from averaging or further trainable layers that do not preserve the generality of the pre-trained features.

**DINO Representations Self-Distillation with No Labels** (DINO) [9] representations are trained in a self-supervised framework. ViTs trained using DINO can do foreground-background segmentation through the attention mask of specific attention heads [9], and can embed part-based semantic information [10]. DINO ViTs also provide higher feature map resolution when compared to CNN-based architectures, which allows finer-grained localization of the part-semantic features [10], a valuable advantage for downstream robot policies. In Figure 1, we show the zero-shot part-semantic abilities of DINO patch embeddings. For each object, we display a heatmap for the cosine similarity between its ViT DINO patch descriptors and the ViT DINO patch descriptor of a reference object a) Mug A, marked with a red dot. Although these images were previously unseen, ViT DINO

extracts representations which locate similar semantic parts of objects.

Our method leverages these rich patch-level embeddings, with minimal processing or further learning on top of the frozen representation to preserve both its generality and easy localization to specific patches in the input image, to obtain policies trained through IL that generalize across object classes.

**Behaviour Cloning** Behaviour Cloning (BC) learns a mapping  $\pi_\theta$  from the current state  $s$  to an action  $a$ :  $\pi_\theta(s) = a$ , that minimizes a regression loss on the training dataset  $D_E$  of expert demonstration state-action tuples  $(s_E, a_E)$ :

$$\operatorname{argmin}_\theta \mathbb{E}_{(s_E, a_E) \sim D_E} \|\pi(s_E) - a_E\|^2. \quad (1)$$

When used with various sensor modalities, each modality can be encoded separately and ultimately fed into the policy as part of the state input. For image inputs specifically, the images are first embedded through a visual backbone and the image representations, flattened and concatenated with the rest of the state variables for input to the policy.

### IV. METHOD

To benefit from the localized semantic descriptors of DINO, our framework processes the features into 2D keypoints for each input image before feeding them to the BC policy. Boiling down the dense visual representation into localized keypoints has two advantages, i) it significantly reduces the input size into the imitation policy, ii) removes the possibility of any overfitting to specific DINO features with the downstream policy, preserving the generality of the pre-trained backbone features. A schematic of our pipeline is displayed in Figure 2.

**Reference Features Initialization** In order to abstract DINO patch embeddings into 2D keypoints, the embeddings extracted from the expert demonstrations are first clustered into a set of reference cluster centroids, each representing a semantic concept present in the demonstration trajectories. The keypoint coordinates are then computed as the locations of the closest feature patch relative to each cluster centroid.

We first extract the  $N \times N$  grid of DINO image patch descriptors as described in section III, from the dataset of all  $J$  images from the expert demonstrations. Treating the resulting  $J \times N^2$  extracted patch embeddings as a bag of features (disregarding their image location, sequence location, or which object), we use K-Means to cluster the set of all embeddings to  $M$  candidate clusters and associated cluster centroids.

To keep only salient clusters found in most demonstration images, we use the voting system and saliency defined by Amir et al. [10]. Formally, let  $a_i^I$  denote the mean [CLS] token attention of the MHSA heads in the last layer of the ViT for patch  $i$  in image  $I$ . Let  $S_j^I$  be the set of all patches in image  $I$  belonging to the  $j$ -th cluster candidate. The saliency for  $S_j^I$  is the average attention value of patches in  $S_j^I$ :

$$\operatorname{sal}(S_j^I) = \frac{1}{|S_j^I|} \sum_{i \in S_j^I} a_i^I. \quad (2)$$

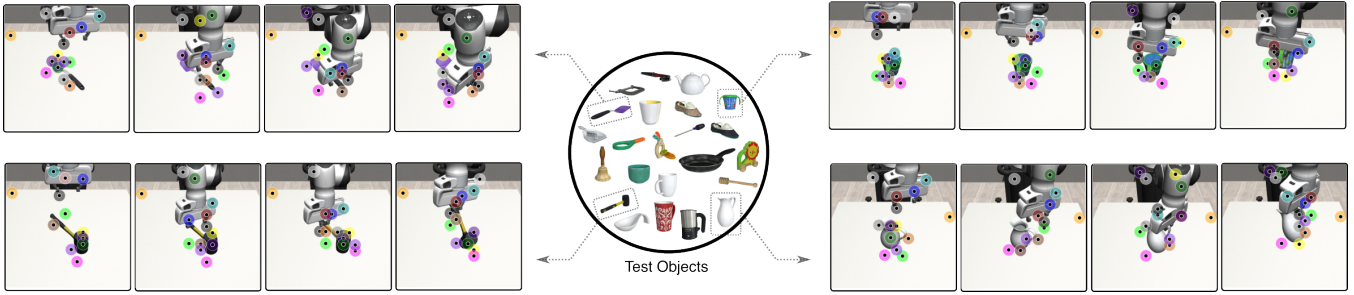


Fig. 3: **Example grasping rollouts on a test set of unseen objects.** Our keypoints (represented by colored circles) track semantic concepts extracted from the expert demonstrations.

Iterating over all the images, a vote is cast by image  $I$  for a given cluster candidate  $C_j$ ,  $0 < j < M$  if the saliency of this cluster in the image exceeds a threshold value  $\tau$ :  $\text{sal}(S_j^I) > \tau$ . Ranking the cluster candidates by votes, we then keep a portion  $m \leq M$  of the most voted for clusters, saving their reference centroids as the set  $F = \{f_0, \dots, f_{m-1}\}$ .

**Keypoint Extraction** Once this initialization procedure is performed, we extract keypoints from subsequent images. For each frame input to the policy we extract its DINO features  $H = \{h_{(x_i, y_j)}\}_{i=1, j=1}^{N, N}$  and compute output vector  $O$  composed of  $m$  image coordinates  $O = (x_k, y_k)_{k=1}^m$ , corresponding to the coordinates of the closest patch DINO feature in the current frame to each of the reference centroids:

$$(x_k, y_k) = \underset{(x_i, y_j)}{\operatorname{argmin}} \frac{f_k \cdot h_{(x_i, y_j)}}{\|f_k\| \|h_{(x_i, y_j)}\|}. \quad (3)$$

This output vector of image coordinates  $O$  forms the visual representation input to the policy head. This procedure allows our approach to track a set of representative DINO semantic concepts extracted from the demonstration image dataset, and outputs the location of the closest available patch feature if this semantic concept is not in the current frame.

In Figure 3 we provide an example of the extracted keypoints obtained using our approach, which track various elements in the rollouts, such as specific parts of the gripper, objects (handle, tip), or fixtures of the environment (e.g. the corner of the table).

## V. GRASPING GENERALIZATION BENCHMARK

To evaluate the generalization abilities of manipulation policies, we develop a benchmark based on a subset of 24 objects from the Google Scanned Objects Dataset [11], a dataset of high quality photorealistic 3D-scanned household objects made for manipulation. Example objects are displayed in Figure 1, and the full set, in Figure 3. The subset was selected to represent a wide range of manipulation difficulty as well as present a range of transfer potential of the manipulation policies among the objects.

Our benchmark covers two focuses. *Intra-class* generalization, where the agent is trained and tested on the same class of objects, with variations in shape and appearance. *Inter-class* generalization, where the agent is tested on a new class of objects which are unseen during training.

**Task** Each task consists of a single object, set on a table in front of the manipulator, where the Panda manipulator must grasp and lift the object. All tasks are simulated in Robosuite [40], where the agent has access to the proprioceptive state of the arm itself but relies on camera inputs to perceive the object. In line with prior work showcasing its benefits in manipulation [15], all methods operate using an end-effector positional Operational Space Controller (OSC) [41], [42].

**Demonstrations** To learn the manipulation policy, the agent has access to a dataset of expert demonstrations, which are collected by an operator through teleoperation using a spacemouse in the Robosuite environments. The training dataset (which varies for each of the benchmarks) consists of 60 demonstration trajectories for each of the objects in the dataset, and will be released alongside our code.

Once a policy is trained to manipulate the objects seen in the training dataset, we evaluate it on a set of unseen test objects by rolling out the policy to accomplish the same task shown in training, only with the new test objects.

**Intra-Class Generalization Benchmark** We use all four mugs available in the Google Scanned objects dataset as our training objects, as they exhibit different looks and shapes but are from the same class. The demonstrated task consists of grasping the mug by its handle and lifting it off the table. To assess the generalization of the trained policies in this context, we employ a leave-one-out cross-validation scheme, forming four splits of three training objects and one object reserved for testing in each split. The test set is therefore always an object of the same class but with an unseen shape and appearance.

**Inter-Class Generalization Benchmark** In order to test the ability of the trained policies to generalize outside the classes of objects shown in training, we choose a training split of three diverse objects: a yellow mug, a pan, and a screwdriver. All other 21 objects shown in Figure 3 are then used as the test set of objects of unseen shapes and appearance, posing a wide range of manipulation difficulty, morphology, and object classes, with objects: of the same semantic parent class (tools, liquid containers) that share similar design features (straight handles and side handles), and objects of entirely different classes with differing degrees of handle-like appendages (basket, toys, shoes with shoetree).

Dataset	Object	Method								
		BC-ViT (Ours)	BC <sub>dino</sub>	BC-RNN <sub>dino</sub>	BC <sub>base</sub>	BC-RNN <sub>base</sub>	BC	BC-RNN	MVP	R3M
Train	Mug (A, B, C)	56.9 ± 6.3	43.1 ± 7.4	68.0 ± 4.1	43.3 ± 1.4	<b>69.3</b> ± 4.7	44.4 ± 2.6	42.4 ± 5.2	35.6 ± 4.4	46.7 ± 2.9
Test	Mug D	<b>63.3</b> ± 9.4	7.3 ± 1.9	16.7 ± 6.6	16.7 ± 6.2	31.3 ± 5.0	47.3 ± 3.4	37.3 ± 5.7	6.0 ± 2.8	6.0 ± 4.9
Train	Mug (A, B, D)	62.0 ± 2.4	41.1 ± 4.6	<b>72.4</b> ± 1.7	50.2 ± 5.1	70.0 ± 6.4	51.3 ± 2.5	45.1 ± 6.5	37.8 ± 7.0	48.9 ± 4.6
Test	Mug C	<b>46.7</b> ± 9.0	26.0 ± 5.9	40.0 ± 4.9	12.7 ± 8.2	24.0 ± 0.0	40.0 ± 4.3	29.3 ± 12.4	0.7 ± 0.9	6.7 ± 3.4
Train	Mug (B, C, D)	61.8 ± 2.5	45.8 ± 6.7	<b>75.3</b> ± 2.4	48.2 ± 5.5	72.0 ± 1.4	53.6 ± 5.4	46.7 ± 4.9	33.1 ± 6.0	50.7 ± 3.4
Test	Mug A	<b>44.0</b> ± 7.5	8.7 ± 6.2	32.0 ± 4.9	0.7 ± 0.9	6.7 ± 3.8	14.0 ± 4.3	14.7 ± 3.4	9.3 ± 6.8	0.0 ± 0.0
Train	Mug (A, C, D)	61.8 ± 1.4	48.4 ± 4.9	69.6 ± 1.4	48.0 ± 4.1	<b>70.4</b> ± 4.1	48.4 ± 5.5	42.2 ± 9.3	43.3 ± 6.6	45.8 ± 3.5
Test	Mug B	<b>28.7</b> ± 5.2	16.7 ± 2.5	<b>28.7</b> ± 5.0	12.0 ± 4.9	22.0 ± 9.1	23.3 ± 5.2	6.7 ± 3.8	3.3 ± 0.9	0.0 ± 0.0
Train Avg.		60.6 ± 2.5	44.6 ± 4.5	<b>71.3</b> ± 1.9	47.4 ± 2.9	70.4 ± 3.4	49.4 ± 2.3	44.1 ± 4.4	37.4 ± 2.6	48.0 ± 1.0
Out-Of-Distribution Avg.		<b>45.7</b> ± 1.7	14.7 ± 2.1	29.3 ± 1.5	10.5 ± 1.1	21.0 ± 1.1	31.2 ± 1.4	22.0 ± 2.0	4.8 ± 0.8	3.2 ± 1.6

TABLE I: Task success rate on intra-class generalization experiment. Results shown are the average of 3 random seeds, with 50 evaluations each, with  $\pm$  standard deviation.

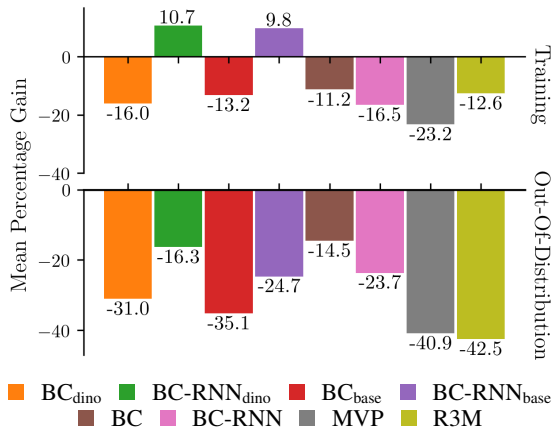


Fig. 4: **Training and out-of-distribution performance on the intra-class generalization experiment.** Our method, BC-ViT consistently improves the average success rate by a minimum of 15% on previously unseen objects.

## VI. RESULTS

Our experiments examine the extent to which robotic policies trained through BC can generalize to changes in object shapes and appearances. We first focus on the ability of policies to generalize in the intra-class case, within the class of objects seen in training but with unseen shapes and appearances. We then examine the inter-class generalization case, testing the transfer ability of the policies’ to objects of various classes, all of unseen shapes and appearances.

**Baselines** We adopt as baselines state-of-the-art methods commonly used in manipulation [15], as well as state-of-the-art representation pre-training methods for IL [7], [8]. We include state-of-the-art approaches for manipulation using BC introduced in [15]: BC and BC<sub>base</sub>. BC uses a randomly initialized visual encoder trained from scratch along the policy head, and BC<sub>base</sub> uses a frozen visual encoder pre-trained on Imagenet [25] with a supervised classification loss. We also add our own baseline, BC<sub>dino</sub> which uses a frozen visual encoder pre-trained on Imagenet with a DINO self-supervised loss, forming the ResNet counterpart to our approach. For each of these three encoder formulations we also consider their mirrored RNN versions: BC-RNN, BC-RNN<sub>base</sub>, and BC-RNN<sub>dino</sub>. BC variants use a standard Multi Layer Perceptron (MLP) policy head, while BC-RNN

[15] variants uses a Recurrent Neural Network (RNN) into a Gaussian Mixture Model policy head. All BC/BC-RNN methods use a Spatial Softmax layer at the outputs of the visual backbones for its performance and generalization benefits [20] and a ResNet-50 backbone for fair comparison as it is the closest ResNet variant in number of weights relative to the variant of ViT used in BC-ViT, ViT-S (21M weights for ViT-S vs 23M for ResNet-50).

We also consider state-of-the-art pre-trained representations from [7] and [8] that have been shown to benefit IL performance, R3M and MVP. We use the ResNet-50 variant of R3M with no changes from its original formulation, feeding flattened convolutional features into an MLP. MVP [8] also follows its original formulation, using the [CLS] token output of a ViT Masked Auto Encoder pre-trained on ImageNet as input to an MLP policy head.

**Evaluation** In alignment with the methodology of [15] we train the visuomotor policies for 600 epochs, rolling out in the training environment every 20 epochs and use the weights of the policy that performs best on the training environment for evaluation. Our evaluation then consists of 50 rollouts for each test environment, rotating the test object in the environment to cover 360 degrees.

### A. Intra-Class Generalization

We first study the capacity of BC policies to generalize to objects within the same class as the expert demonstrations while varying shapes and appearances, testing the ability of trained policies to abstract visual semantics from the training dataset to novel, unseen objects of the same class.

While easier than inter-class generalization, the intra-class setting is challenging as the demonstrations only show a very specific behaviour that lifts the mugs from their handle, making it a behaviour that requires a degree of precision, with variations based on the width, height, and handle shape of the mug in question. Results are reported in Table I and Figure 4 for each train-validation split.

**Discussion** BC-ViT consistently outperforms all baselines on the test set objects, showing superior out-of-distribution generalization, while BC-RNN<sub>dino</sub> performs best on the training objects, showing the advantage of using DINO pretrained features for either contexts. Notably, BC performs surprisingly well in the out-of-distribution context, on par with

Dataset Object		Method								
		BC-ViT (Ours)	BC <sub>dino</sub>	BC-RNN <sub>dino</sub>	BC <sub>base</sub>	BC-RNN <sub>base</sub>	BC	BC-RNN	MVP	R3M
Train	Mug D	52.0 ± 2.8	38.0 ± 5.7	69.3 ± 6.2	37.3 ± 4.1	<b>70.7</b> ± 7.7	43.3 ± 6.6	30.7 ± 11.8	39.3 ± 3.4	47.3 ± 0.9
	Pan	83.3 ± 2.5	69.3 ± 6.8	<b>89.3</b> ± 3.4	71.3 ± 6.2	88.7 ± 2.5	69.3 ± 3.4	71.3 ± 5.0	60.0 ± 5.9	68.7 ± 5.0
	Screwdriver	<b>91.3</b> ± 2.5	73.3 ± 5.2	<b>91.3</b> ± 5.2	66.7 ± 2.5	89.3 ± 1.9	87.3 ± 3.4	76.0 ± 7.1	59.3 ± 5.7	79.3 ± 5.2
Test	Mug A	<b>47.3</b> ± 0.9	10.0 ± 2.8	3.3 ± 3.4	6.0 ± 0.0	11.3 ± 1.9	20.0 ± 4.3	8.0 ± 5.9	9.3 ± 4.1	0.0 ± 0.0
	Mug B	30.0 ± 5.7	8.7 ± 1.9	21.3 ± 2.5	4.7 ± 2.5	14.0 ± 1.6	<b>32.0</b> ± 11.4	19.3 ± 3.8	7.3 ± 2.5	4.0 ± 3.3
	Mug C	24.7 ± 3.8	14.0 ± 3.3	15.3 ± 5.2	4.7 ± 1.9	9.3 ± 3.4	<b>40.7</b> ± 4.7	19.3 ± 5.7	8.0 ± 2.8	2.0 ± 1.6
	Teapot	14.0 ± 5.9	4.0 ± 1.6	<b>15.3</b> ± 3.4	4.0 ± 3.3	3.3 ± 0.9	5.3 ± 0.9	0.0 ± 0.0	0.0 ± 0.0	0.0 ± 0.0
	Pitcher	8.0 ± 4.3	1.3 ± 0.9	4.0 ± 4.3	3.3 ± 0.9	4.7 ± 2.5	<b>10.7</b> ± 9.6	7.3 ± 4.1	5.3 ± 2.5	6.7 ± 3.8
	Coffee	<b>8.7</b> ± 3.4	8.0 ± 3.3	8.0 ± 4.9	3.3 ± 1.9	6.0 ± 3.3	8.0 ± 3.3	4.7 ± 2.5	7.3 ± 3.8	2.7 ± 2.5
	Kidcup	<b>10.0</b> ± 3.3	2.0 ± 1.6	4.7 ± 6.6	4.0 ± 5.7	0.7 ± 0.9	6.0 ± 1.6	2.7 ± 2.5	0.0 ± 0.0	0.0 ± 0.0
	Hammer	50.7 ± 4.1	48.7 ± 10.9	<b>66.7</b> ± 4.1	42.7 ± 5.7	62.7 ± 9.3	58.7 ± 4.7	48.7 ± 5.0	16.0 ± 2.8	19.3 ± 5.7
	Spatula	58.7 ± 9.3	35.3 ± 0.9	43.3 ± 10.9	14.7 ± 4.1	32.7 ± 3.8	<b>72.7</b> ± 3.4	62.0 ± 5.9	20.0 ± 2.8	0.0 ± 0.0
	Mag. Glass	<b>28.7</b> ± 1.9	0.7 ± 0.9	2.7 ± 0.9	4.7 ± 0.9	11.3 ± 5.2	14.0 ± 5.9	2.0 ± 2.8	6.0 ± 4.3	0.0 ± 0.0
	Hair Straightener	50.0 ± 4.3	14.7 ± 0.9	18.0 ± 7.5	28.7 ± 8.4	32.7 ± 6.8	<b>55.3</b> ± 9.4	37.3 ± 5.2	18.0 ± 2.8	8.0 ± 3.3
	Spoonrest	51.3 ± 10.9	38.0 ± 5.9	<b>56.7</b> ± 5.0	27.3 ± 3.4	43.3 ± 5.2	38.0 ± 4.3	10.7 ± 6.2	4.7 ± 2.5	0.0 ± 0.0
	DustPan	<b>32.0</b> ± 5.7	25.3 ± 1.9	29.3 ± 2.5	9.3 ± 5.0	22.7 ± 3.4	18.7 ± 7.7	8.0 ± 3.3	2.0 ± 2.8	0.0 ± 0.0
	Basket	16.0 ± 2.8	12.7 ± 8.4	4.0 ± 5.7	12.0 ± 7.5	<b>18.7</b> ± 6.2	16.0 ± 5.9	6.0 ± 8.5	0.7 ± 0.9	0.7 ± 0.9
	Bell	<b>30.0</b> ± 10.2	15.3 ± 4.7	12.7 ± 9.0	6.7 ± 0.9	22.0 ± 8.6	22.0 ± 13.4	28.7 ± 14.8	20.7 ± 3.8	1.3 ± 0.9
	C-Clamp	5.3 ± 4.1	10.0 ± 5.9	14.0 ± 4.3	2.7 ± 3.8	<b>21.3</b> ± 9.0	20.7 ± 2.5	6.7 ± 5.0	7.3 ± 2.5	3.3 ± 0.9
	Honeydip	2.7 ± 2.5	16.7 ± 10.5	<b>26.7</b> ± 16.4	16.7 ± 6.2	6.7 ± 5.2	2.7 ± 1.9	4.0 ± 5.7	0.7 ± 0.9	0.7 ± 0.9
	Shoe1	<b>30.0</b> ± 2.8	24.7 ± 9.6	27.3 ± 6.8	20.0 ± 3.3	21.3 ± 6.6	24.0 ± 5.9	10.0 ± 4.9	9.3 ± 4.7	1.3 ± 0.9
	Shoe2	28.0 ± 5.7	22.0 ± 1.6	<b>42.0</b> ± 7.1	13.3 ± 4.1	26.0 ± 5.9	17.3 ± 2.5	10.0 ± 3.3	11.3 ± 4.1	0.0 ± 0.0
Rattle	<b>45.3</b> ± 13.9	12.7 ± 1.9	13.3 ± 6.6	14.0 ± 8.5	16.0 ± 4.9	24.0 ± 8.2	13.3 ± 10.5	2.7 ± 0.9	8.0 ± 2.8	
Lion Toy	<b>20.7</b> ± 4.7	2.7 ± 2.5	4.0 ± 4.3	18.7 ± 7.7	9.3 ± 0.9	16.0 ± 4.3	4.0 ± 1.6	4.0 ± 2.8	0.7 ± 0.9	
Train Avg.	75.6 ± 1.7	60.2 ± 5.5	<b>83.3</b> ± 3.4	58.4 ± 2.1	82.9 ± 2.1	66.7 ± 2.2	59.3 ± 4.3	52.9 ± 1.7	65.1 ± 1.7	
Out-Of-Distribution Avg.	<b>28.2</b> ± 1.9	15.6 ± 0.5	20.6 ± 3.7	12.4 ± 1.0	18.9 ± 1.2	24.9 ± 0.7	14.9 ± 1.6	7.7 ± 1.2	2.8 ± 0.4	

TABLE II: Task success rate on the inter-class generalization experiment. Results shown are the average of 3 random seeds, with 50 evaluations each, with  $\pm$  standard deviation.

BC-RNN<sub>dino</sub>, showing that learning a representation from scratch is competitive with other CNN-based approaches, although still 15% behind BC-ViT in average success rate. The representation learning-based baselines, MVP and R3M, perform poorly on the unseen objects.

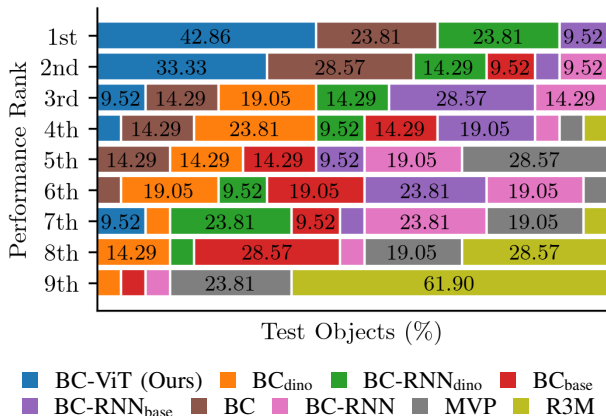


Fig. 5: **Ranking of methods on the 21 out-of-distribution objects of the inter-class generalization experiment.** The length of the bar represents the percentage of test objects each method ranked 1<sup>st</sup> – 9<sup>th</sup>. BC-ViT leads the studied methods, performing best on 42% of the previously unseen test set objects, and 2<sup>nd</sup> or 3<sup>rd</sup> best for most other objects

### B. Inter-Class Generalization

We next study the inter-class generalization setting. The inter-class poses a more difficult challenge than the previous setting as the test objects may no longer share physical characteristics or appearance with the objects found in the training dataset of demonstrations. Our results are reported in Table II and aggregated in Figure 5.

**Discussion** We find that BC-ViT outperforms all other methods on this difficult test set and BC-RNN<sub>dino</sub> leads performance on the seen objects, showing the positive effect of using DINO features. BC-ViT, as shown in Figure 5, consistently ranks ahead of competing methods, outperforming all methods on 42% of the unseen test objects, and placing second best or third on most other objects. Surprisingly, BC performs second best in out-of-distribution (OOD) tasks, showing that when shown with a diverse set of training objects, training using a BC loss only can lead to learning representations that transfer well between objects.

## VII. CONCLUSION

In this paper we aim to evaluate and improve the generalization properties of imitation learning systems. We introduce a benchmark based on the Google Scanned Objects dataset [11] and the Panda manipulator simulation in Robosuite [40], alongside a dataset of expert demonstrations. This benchmark evaluates intra-class variations such as color or shape, as well as major inter-class semantic differences between training and test data.

To tackle our benchmark, we present BC-ViT, an IL framework that leverages dense DINO features abstracted into image keypoints as the visual representation for visual BC. In our evaluation of BC-ViT’s ability for out-of-distribution generalization, we find that it consistently surpasses the performance of existing state-of-the-art methods.

BC-ViT highlights the potential of stable semantic representations to ground robotic behaviour. Our keypoints track critical features on all of the gripper, target object and background, enabling zero-shot adaptation to unseen objects – a step towards robots with more human-like manipulation.

## REFERENCES

- [1] P. Abbeel and A. Y. Ng, "Apprenticeship learning via inverse reinforcement learning," in *Proceedings of the twenty-first international conference on Machine learning*. ACM, 2004, p. 1.
- [2] J. Ho and S. Ermon, "Generative adversarial imitation learning," in *Advances in Neural Information Processing Systems*, 2016, pp. 4565–4573.
- [3] W.-D. Chang, J. C. G. Higuera, S. Fujimoto, D. Meger, and G. Dudek, "Il-flow: Imitation learning from observation using normalizing flows," *arXiv preprint arXiv:2205.09251*, 2022.
- [4] P. Florence, C. Lynch, A. Zeng, O. A. Ramirez, A. Wahid, L. Downs, A. Wong, J. Lee, I. Mordatch, and J. Tompson, "Implicit behavioral cloning," in *Conference on Robot Learning*. PMLR, 2022, pp. 158–168.
- [5] C. Chi, S. Feng, Y. Du, Z. Xu, E. Cousineau, B. Burchfiel, and S. Song, "Diffusion policy: Visuomotor policy learning via action diffusion," in *Proceedings of Robotics: Science and Systems (RSS)*, 2023.
- [6] S. Parisi, A. Rajeswaran, S. Purushwalkam, and A. Gupta, "The unsurprising effectiveness of pre-trained vision models for control," in *International Conference on Machine Learning, ICML 2022*, 2022.
- [7] S. Nair, A. Rajeswaran, V. Kumar, C. Finn, and A. Gupta, "R3M: A universal visual representation for robot manipulation," in *Conference on Robot Learning, CoRL 2022, 14-18 December 2022, Auckland, New Zealand*, ser. Proceedings of Machine Learning Research, vol. 205. PMLR, 2022, pp. 892–909.
- [8] T. Xiao, I. Radosavovic, T. Darrell, and J. Malik, "Masked visual pre-training for motor control," *arXiv:2203.06173*, 2022.
- [9] M. Caron, H. Touvron, I. Misra, H. Jégou, J. Mairal, P. Bojanowski, and A. Joulin, "Emerging properties in self-supervised vision transformers," in *Proceedings of the IEEE/CVF international conference on computer vision*, 2021, pp. 9650–9660.
- [10] S. Amir, Y. Gandselman, S. Bagon, and T. Dekel, "Deep vit features as dense visual descriptors," *arXiv preprint arXiv:2112.05814*, vol. 2, no. 3, p. 4, 2021.
- [11] L. Downs, A. Francis, N. Koenig, B. Kinman, R. Hickman, K. Reymann, T. B. McHugh, and V. Vanhoucke, "Google scanned objects: A high-quality dataset of 3d scanned household items," in *2022 International Conference on Robotics and Automation (ICRA)*. IEEE, 2022, pp. 2553–2560.
- [12] D. A. Pomerleau, "Efficient training of artificial neural networks for autonomous navigation," *Neural computation*, vol. 3, no. 1, pp. 88–97, 1991.
- [13] R. Rahmatizadeh, P. Abolghasemi, L. Bölöni, and S. Levine, "Vision-based multi-task manipulation for inexpensive robots using end-to-end learning from demonstration," in *2018 IEEE international conference on robotics and automation (ICRA)*. IEEE, 2018, pp. 3758–3765.
- [14] P. Florence, L. Manuelli, and R. Tedrake, "Self-supervised correspondence in visuomotor policy learning," *IEEE Robotics and Automation Letters*, vol. 5, no. 2, pp. 492–499, 2019.
- [15] A. Mandlekar, D. Xu, J. Wong, S. Nasiriany, C. Wang, R. Kulkarni, L. Fei-Fei, S. Savarese, Y. Zhu, and R. Martín-Martín, "What matters in learning from offline human demonstrations for robot manipulation," in *Conference on Robot Learning (CoRL)*, 2021.
- [16] S. Ross, G. Gordon, and D. Bagnell, "A reduction of imitation learning and structured prediction to no-regret online learning," in *Proceedings of the fourteenth international conference on artificial intelligence and statistics*. JMLR Workshop and Conference Proceedings, 2011, pp. 627–635.
- [17] C. Wang, R. Wang, A. Mandlekar, L. Fei-Fei, S. Savarese, and D. Xu, "Generalization through hand-eye coordination: An action space for learning spatially-invariant visuomotor control," in *2021 IEEE/RSJ International Conference on Intelligent Robots and Systems (IROS)*. IEEE, 2021, pp. 8913–8920.
- [18] H. Kim, Y. Ohmura, and Y. Kuniyoshi, "Gaze-based dual resolution deep imitation learning for high-precision dexterous robot manipulation," *IEEE Robotics and Automation Letters*, vol. 6, no. 2, pp. 1630–1637, 2021.
- [19] T. Yu, C. Finn, A. Xie, S. Dasari, T. Zhang, P. Abbeel, and S. Levine, "One-shot imitation from observing humans via domain-adaptive meta-learning," *arXiv preprint arXiv:1802.01557*, 2018.
- [20] S. Levine, C. Finn, T. Darrell, and P. Abbeel, "End-to-end training of deep visuomotor policies," *Journal of Machine Learning Research*, vol. 17, no. 39, pp. 1–40, 2016. [Online]. Available: <http://jmlr.org/papers/v17/15-522.html>
- [21] M. Laskin, A. Srinivas, and P. Abbeel, "Curl: Contrastive unsupervised representations for reinforcement learning," in *International Conference on Machine Learning*. PMLR, 2020, pp. 5639–5650.
- [22] D. Yarats, I. Kostrikov, and R. Fergus, "Image augmentation is all you need: Regularizing deep reinforcement learning from pixels," in *International Conference on Learning Representations*, 2021. [Online]. Available: <https://openreview.net/forum?id=GY6-6sTvGaf>
- [23] D. Yarats, R. Fergus, A. Lazaric, and L. Pinto, "Mastering visual continuous control: Improved data-augmented reinforcement learning," in *International Conference on Learning Representations*, 2021.
- [24] S. Fujimoto, W.-D. Chang, E. J. Smith, S. S. Gu, D. Precup, and D. Meger, "For sale: State-action representation learning for deep reinforcement learning," *arXiv preprint arXiv:2306.02451*, 2023.
- [25] J. Deng, W. Dong, R. Socher, L.-J. Li, K. Li, and L. Fei-Fei, "Imagenet: A large-scale hierarchical image database," in *2009 IEEE Conference on Computer Vision and Pattern Recognition*, 2009, pp. 248–255.
- [26] K. Grauman, A. Westbury, E. Byrne, Z. Chavis, A. Furnari, R. Girdhar, J. Hamburger, H. Jiang, M. Liu, X. Liu *et al.*, "Ego4d: Around the world in 3,000 hours of egocentric video," in *Proceedings of the IEEE/CVF Conference on Computer Vision and Pattern Recognition*, 2022, pp. 18995–19012.
- [27] J. Tobin, R. Fong, A. Ray, J. Schneider, W. Zaremba, and P. Abbeel, "Domain randomization for transferring deep neural networks from simulation to the real world," in *2017 IEEE/RSJ international conference on intelligent robots and systems (IROS)*. IEEE, 2017, pp. 23–30.
- [28] F. Sadeghi, A. Toshev, E. Jang, and S. Levine, "Sim2real viewpoint invariant visual servoing by recurrent control," in *Proceedings of the IEEE Conference on Computer Vision and Pattern Recognition*, 2018, pp. 4691–4699.
- [29] D. Wang, C. Devin, Q.-Z. Cai, F. Yu, and T. Darrell, "Deep object-centric policies for autonomous driving," in *2019 International Conference on Robotics and Automation (ICRA)*. IEEE, 2019, pp. 8853–8859.
- [30] C. Devin, P. Abbeel, T. Darrell, and S. Levine, "Deep object-centric representations for generalizable robot learning," in *2018 IEEE International Conference on Robotics and Automation (ICRA)*. IEEE, 2018, pp. 7111–7118.
- [31] M. Sieb, Z. Xian, A. Huang, O. Kroemer, and K. Fragkiadaki, "Graph-structured visual imitation," in *Conference on Robot Learning*. PMLR, 2020, pp. 979–989.
- [32] Y. Zhu, A. Joshi, P. Stone, and Y. Zhu, "Viola: Object-centric imitation learning for vision-based robot manipulation," in *Conference on Robot Learning*. PMLR, 2023, pp. 1199–1210.
- [33] J. Tremblay, T. To, B. Sundaralingam, Y. Xiang, D. Fox, and S. Birchfield, "Deep object pose estimation for semantic robotic grasping of household objects," *arXiv preprint arXiv:1809.10790*, 2018.
- [34] G. Du, K. Wang, S. Lian, and K. Zhao, "Vision-based robotic grasping from object localization, object pose estimation to grasp estimation for parallel grippers: a review," *Artificial Intelligence Review*, vol. 54, no. 3, pp. 1677–1734, 2021.
- [35] X. Wang, H. Kang, H. Zhou, W. Au, and C. Chen, "Geometry-aware fruit grasping estimation for robotic harvesting in apple orchards," *Computers and Electronics in Agriculture*, vol. 193, p. 106716, 2022.
- [36] P. R. Florence, L. Manuelli, and R. Tedrake, "Dense object nets: Learning dense visual object descriptors by and for robotic manipulation," in *Conference on Robot Learning*. PMLR, 2018, pp. 373–385.
- [37] J. D. M.-W. C. Kenton and L. K. Toutanova, "Bert: Pre-training of deep bidirectional transformers for language understanding," in *Proceedings of NAACL-HLT*, 2019, pp. 4171–4186.
- [38] L. Beyer, X. Zhai, and A. Kolesnikov, "Better plain vit baselines for imagenet-1k," *arXiv preprint arXiv:2205.01580*, 2022.
- [39] C. Renggli, A. S. Pinto, N. Houlsby, B. Mustafa, J. Puigcerver, and C. Riquelme, "Learning to merge tokens in vision transformers," *arXiv preprint arXiv:2202.12015*, 2022.
- [40] Y. Zhu, J. Wong, A. Mandlekar, R. Martín-Martín, A. Joshi, S. Nasiriany, and Y. Zhu, "robosuite: A modular simulation framework and benchmark for robot learning," in *arXiv preprint arXiv:2009.12293*, 2020.
- [41] O. Khatib, "A unified approach for motion and force control of robot manipulators: The operational space formulation," *IEEE Journal on Robotics and Automation*, vol. 3, no. 1, pp. 43–53, 1987.
- [42] J. Peters and S. Schaal, "Learning operational space control." in *Robotics: Science and Systems*, vol. 10, 2006.